Temporal Instanton Analysis: Development and Implementation

Jonas Kersulis, Ian Hiskens
Elec. Eng. and Computer Science
University of Michigan
Ann Arbor, MI, United States

Michael Chertkov, Scott Backhaus
Center for Nonlinear Studies
Los Alamos National Laboratory
Los Alamos, NM, United States

Daniel Bienstock
Ind. Eng. and Operations Research
Columbia University
New York, NY, United States

***Abstract*—A previously-developed method for studying a transmission network's vulnerability to wind forecast inaccuracy is expanded. This method uses optimization to find a wind generation pattern close to the forecast that violates a specified line. Repeating the optimization for all lines in the network yields a set of generation patterns which may be sorted by likelihood. Instanton analysis thus yields insight into the potential effects of wind forecast inaccuracy at the system level.**

***Index Terms*—Forecast uncertainty, Optimization, Transmission operations, Wind energy**

I. Introduction and review

The impact of wind forecast inaccuracy is greater than ever in grids around the world. As reliance on wind generation increases, changes in weather can induce network congestion. In certain cases this congestion may even cause a transmission line to overheat and sag. System operators use wind forecast data to steer the network away from these scenarios, but wind forecasts are significantly less accurate than generation and demand predictions. How might forecast inaccuracies compound across the network to overheat transmission lines? How likely is this to occur? Temporal instanton analysis helps answer these questions by identifying troublesome wind patterns and ranking them according to likelihood. With this information, system operators and planners may better prepare for renewable generation uncertainty.

The instanton problem was initially considered in [1] and [2] where a DC power flow approximation was used to turn instanton analysis into a convex problem with an analytic solution. The physically accurate AC power flow formulation was used in [3], with an iterative scheme required for finding instanton candidates. Current instanton research is exploring the tradeoff between problem complexity and solution accuracy, with the goal of developing the most accurate model that remains convex (and therefore guarantees a solution). Instanton work to date has focused on instantaneous vulnerability by seeking to find the smallest wind generation change that drives a line to its power or current limit. Thus, the troublesome wind patterns uncovered by such instanton analysis may be fleeting.

It is safe to temporarily operate a line above its current limit. Transmission system operators know this and periodically allow lines to operate above their limits to promote smooth operation under heavy, though temporary, flow patterns (see the introduction of [4] for a history of dynamic line rating starting in the 1970s). It takes time for line conductors to heat sufficiently that they sag to an unacceptable level (as defined by statute and nearby tree limbs). As long as the line is allowed to cool before reaching this point, no harm will be done. If an operator is comfortable with temporarily overloaded lines, information from existing instanton analysis may be too conservative to aid decision making.

In this paper we expound on temporal instanton analysis. The line temperature model we use is derived from [8]. Ohmic loss heating is related to power flow angle differences according to a relationship from [9]. By modeling line temperature over an appropriate time horizon, the proposed method discovers multiple-time-step wind patterns that are both likely to occur and sure to induce excessive sag for at least one line in the network.

The remainder of this paper is organized as follows. Section II describes the models at the core of temporal instanton analysis. Section III combines these models into a quadratically-constrained quadratic program (QCQP). The solution of this QCQP is described in Section IV. Section V contains results for two networks: a modified version of the RTS-96 and the larger WECC network. The former network has been used in previous instanton analysis studies, while the latter serves to demonstrate scalability of temporal instanton analysis. Finally, an appendix contains a detailed description of the thermal model used to calculate line temperature.

We expand on prior work by providing a more detailed treatment of the objective function, discussing implementation details including computational complexity and sparsity, and proposing a particular algorithm for solving the secular equation.

II. Models

The ultimate goal is to find the most likely forecast errors that would cause a line in the network to reach its temperature limit. This goal entwines three phenomena, each with its own model. First, a transmission line's temperature must be modeled using a heat balance equation. Second, forecast error likelihood must be quantified via some statistical

The authors acknowledge the support of the Los Alamos National Laboratory Grid Science Program, subcontract 270958.

model. Finally, an underlying network model delineates the feasible region of network operation. This section describes these three models in detail. The next section combines them into a quadratically-constrained quadratic program, a purely mathematical expression of the temporal instanton analysis goal. A full analysis entails solving this QCQP for each line in the given network.

A. Transmission line heating

Our heating model is derived from [8]. It is a recursive relationship between initial and final line temperatures based on angle differences at all time steps under consideration. The appendix, Section VIII, acts as a bridge between our model and [8].

Consider a time horizon with T intervals, each on the order of ten minutes long. Power flow data is updated after each interval, but all other parameters remain constant. Choose a single transmission line in the network —suppose it lies between nodes i and j— and let this line's thermal limit be represented by T_{lim} (°C). We can constrain the line's temperature at the end of the T-th interval to be equal to this limiting value by enforcing the second-order constraint

$$\sum_{k=1}^{n} \hat{\theta}_{ij}(t_k)^2 = \frac{a}{c}\left(T_{\text{lim}} - f\right), \tag{1}$$

where

- $\hat{\theta}_{ij}(t_k) = \theta_{ij}(t_k)\sqrt{(e^{(t_1-t_0)a})^{n-k+1} - (e^{(t_1-t_0)a})^{n-k}}$
  - $\theta_{ij}(t_k)$ is the angle difference across line ij at time interval t_k.
  - $(t_1 - t_0)$ is the length of each time interval (in seconds).
- $a = \frac{1}{mC_p}\left[-\eta_c - 4\eta_r(T_{\text{mid}} + 273)^3\right]$ is constant with units of s^{-1}.
  - mC_p is the heat capacity, with units of J/m-°C.
  - η_c is the conductive heat loss rate coefficient, with units of W/m-°C.
  - η_r is the conductive heat loss rate coefficient, with units of W/m-°C^4.
  - T_{mid} is the average of ambient temperature T_{amb} and limit temperature T_{lim}, in Celsius.
- $c = \frac{r_{ij}S_b}{3mC_p x_{ij}^2 L_{ij}}$ is a constant with units of W/m.
  - r_{ij} is resistance of line ij in per unit.
  - x_{ij} is reactance of line ij in per unit.
  - S_b is the system base (e.g. 100 MVA).
  - L_{ij} is the length of one phase of line ij, in m.
- f is a constant with units of degrees Celsius, defined to be

$$f = (e^{(t_1-t_0)a})^n T(t_0) + \frac{d}{a}\left[\sum_{i=1}^{n}\left((e^{(t_1-t_0)a})^i - (e^{(t_1-t_0)a})^{i-1}\right)\right]$$

  - $T(t_0)$ is the line's initial temperature (steady state temperature under base case power flow condition)
  - d is a constant with units of W/m, defined to be

$$d = \frac{1}{mC_p}\left[\eta_c T_{\text{amb}} - \eta_r\left((T_{\text{mid}} + 273)^4 - (T_{\text{amb}} + 273)^4\right) + 4\eta_r T_{\text{mid}}(T_{\text{mid}} + 273)^3 + q_s\right],$$

    where q_s is the solar heat gain rate in W/m.

B. Wind forecast inaccuracy

Consider several wind farms scattered across a transmission grid. Each wind site has a forecast power output. Let the error in this forecast be represented by a zero-mean Gaussian random variable.[1] Then for any instant in time, the collection of wind forecast errors across the network takes the form of a Gaussian random vector. Elements of this vector are correlated due to spatial relationships between wind sites: if wind speed increases at one site, for instance, a simultaneous decrease at a neighboring site is unlikely. Temporal instanton analysis considers multiple time steps, which introduces temporal correlation. Increased wind at one site during the current time interval may be correlated with greater wind speed at downwind sites during the following interval. Other sources of uncertainty (e.g. hydro generation, demand) may be considered as readily as wind, but may not exhibit spatial or temporal correlation. Thus, the model we use may be simplified to consider other sources of uncertainty.

Suppose a network has N_R wind sites and we wish to consider T time intervals. Let dev be the $(N_R \cdot T) \times 1$ vector of forecast deviations across all wind sites and time intervals. The first T elements of dev contain forecast errors for the first site at time intervals $1 - T$, the second T elements are errors for the second site, and so on. The probability density function for dev is

$$f(dev) = \frac{\exp\left(-\frac{1}{2}dev^\top \mathbf{C}^{-1} dev\right)}{(2\pi)^{\frac{n}{2}}\sqrt{\det \mathbf{C}}},$$

where $\mathbf{C}$ is the correlation matrix. Maximizing f corresponds to minimizing $dev^\top \mathbf{C}^{-1} dev$. Thus, one may express a desire to maximize wind pattern likelihood with

$$\min \; dev^\top \mathbf{Q} dev,$$

where $\mathbf{Q} = \mathbf{C}^{-1}$ is the precision matrix. There are many ways to determine C or Q from historical data. One example is the method proposed by [7], whose authors use maximum likelihood optimization is used to fit a model with eleven parameters to observed data. The precision matrix produced by this method consists of tridiagonal blocks, and is sparse.

The first step is to encode the spatial layout of the network's wind farms so each site has at most four neighbors: North, South, West, and East. Figure 1 illustrates spatial relationships for our modified RTS-96 network, whose eighteen wind sites are distributed across three uncorrelated areas.

[1] Forecast errors are commonly assumed to be Gaussian, but in reality they are better modeled by Cauchy distributions; see [6].

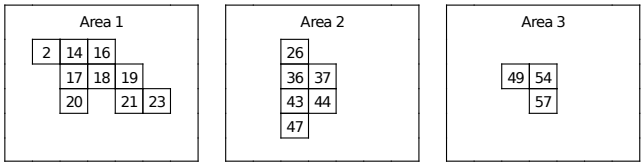

Fig. 1. Wind farm spatial relationships in a modified RTS-96 network. (Note: bus indices have been mapped to 1:73.)

C. Network model

Power balance is ever-present in power systems analyses. Our specific model exhibits two important details. First, it uses the DC power flow approximations. Second, we allow for distributed slack. The mismatch between total power generation and demand at any time step is divided over one or more generators according to generator participation factors. This slack model is more realistic than the single slack bus, which assumes one generator compensates for all mismatch.

The three models described in this section are the three necessary ingredients of temporal instanton analysis. The next section combines them into a QCQP.

III. Temporal instanton QCQP

The following quadratically constrained quadratic program is a concise expression of our desire to find feasible, likely wind patterns that will cause a chosen line in the network to reach its temperature limit by the end of a given time horizon.

$$\min_{dev} \quad \sum_{t=1}^{T} dev_t^\top Q_{dev} dev_t \tag{2a}$$

subject to:

$$\sum_j Y_{ij}\theta_{ij,t} = G_{i,t} + R_{i,t} + dev_{i,t} - D_{i,t} \qquad \forall i \in 1...N,\ t \in 1...T \tag{2b}$$

$$G_t = G_{0,t} + k\alpha_t \qquad \forall t \in 1 \dots T \tag{2c}$$

$$\theta_{ref,t} = 0 \qquad \forall t \in 1 \dots T \tag{2d}$$

$$\Delta T_{ij}[T] = \Delta T_{ij}^{\lim} \qquad \text{for some } (i,j) \in \mathcal{G} \tag{2e}$$

where:

- $dev_{i,t}$ is the difference between actual output and forecast output at wind-farm i and time t. Thus, dev_t is the vector of wind forecast deviations at time t.
- Q_{dev} may be set to the identity matrix or used to covariance between wind sites.
- $R_{i,t}$ is renewable generation forecast at bus i and time t.
- Y_{ij} is the (i,j)-th element of the admittance matrix, which assumes zero resistance.
- $\theta_{ij,t}$ is the difference between voltage angles θ_i and θ_j at time t.
- $G_{i,t}$ is conventional active power generation at node i and time t, and G_t is a vector including all nodes.
- $D_{i,t}$ is active power demand at bus i and time t.
- N is the number of buses (nodes).
- $G_{0,t}$ is scheduled conventional active power generation (without droop response).
- k is the vector of participation factors for conventional generators, with $\sum_i k_i = 1$. (The case where $k_i = 1$ corresponds to generator i taking all slack.)
- α_t is the power mismatch at time t.
- ΔT_{ij}^{lim} is the change in temperature that will push line (i,j) to its thermal limit.
- θ_{ref} is the voltage angle of the reference bus.
- $\mathcal{G}$ is the set of edges (lines).

Equation (2a) expresses the desire to find wind patterns that remain close to the wind forecast. The first constraint equation (2b) enforces DC power balance. The next constraint (2c) models conventional active power generation as a sum of scheduled generation and droop response (where generators share the task of compensating for mismatch between total generation and load). The system angle reference is established by (2d). Last is (2e), which constrains the temperature of a particular line to be equal to its limit at the final time T. Note that (2e) is actually (1), whose details were given separate treatment in Section II-A.

Thus, (2) has a quadratic objective function, a set of linear constraints, and a single quadratic constraint. By solving (2) for each line in the network, we obtain a set of instanton candidate wind patterns, each of which will heat a particular line to its thermal limit. Of these candidates, the one that deviates least from the wind forecast (across all time steps) is the instanton wind pattern. The next section contains a solution method for QCQPs of the form (2), based on work in [10].

IV. Solution method and implementation details

Previous instanton work relied on convex optimization to quickly find instanton wind patterns. Heat-constrained temporal instanton analysis is more complicated: it cannot be formulated as anything simpler than a quadratically-constrained quadratic program (QCQP). QCQPs are NP-hard in general; reasonable solutions may exist, but unless the quadratic constraint matrices are positive-definite there is no solution guarantee (see [12]). Because system operators require robustness, "no solution found" is an unacceptable output. With this criterion in mind, we proceed to develop an optimization model whose structure permits us to find solutions despite nonconvexity.

We can emphasize the QCQP form of (2) by combining all variables into a single vector z and re-writing (2) as a canonical QCQP:

$$\min \quad z_1^\top \mathbf{Q}_z z_1 \tag{3a}$$

$$s.t. \quad \mathbf{A}z = b \tag{3b}$$

$$z_3^\top z_3 = c \tag{3c}$$

The objective (3a) is equivalent to (2a), the linear equality constraints (3b) represent (2b)-(2d), and the quadratic equality constraint (3c) is equivalent to (2e). The vector z consists of $(N+N_R+2)T$ variables, where N is the number of nodes, N_R is the number of nodes with wind-farms, and T is the number

of time steps. Subscripts are used to distinguish variables: $z_1 \in \mathbb{R}^{N_R T}$ contains all wind deviations, $z_2 \in \mathbb{R}^{(N+1)T}$ contains angle and mismatch variables, and $z_3 \in \mathbb{R}^T$ contains auxiliary angle difference variables involved in line temperature calculation. Note that $N_R T$ of the variables represent deviations from forecast at each wind-farm and time step. There are also NT angle variables (of which T are fixed to zero according to (2d)) and T mismatch variables α_t (one per time step). The last T variables are auxiliary angle difference variables used to convert (2e) into a norm constraint.

The structure of (3) is similar to that of the well-known trust region subproblem. Here we describe a four-step solution method based in part on [10]. Several changes of variables may be used to obtain an equivalent form of (3) whose solution is straightforward.

A. Translation

The first step is to change variables from z to $y = z - z^*$, where $z^* \in \{z : Az = b\}$. This translation transforms $Az = b$ into $Ay = 0$. To prevent the change from introducing a linear term into the quadratic constraint, we require $z_3^* = 0$. To satisfy $Az^* = b$, the subvectors z_1^* and z_2^* must satisfy,

$$A \begin{bmatrix} z_1^* \\ z_2^* \\ 0 \end{bmatrix} = b.$$

It is straightforward to find a min-norm z^* that satisfies this constraint by partitioning and factorizing A appropriately. After translation, the problem becomes

$$\begin{aligned} \min \quad & y_1^\top Q_z y_1 + 2 y_1^\top Q_z z_1^* && \text{(4a)} \\ s.t. \quad & Ay = 0 && \text{(4b)} \\ & y_3^\top y_3 = c. && \text{(4c)} \end{aligned}$$

B. Kernel mapping

The form of (4b) suggests an intuitive explanation: any solution to (4) must lie in the nullspace (kernel) of A. If $\dim \mathcal{N}(A) = k$ is the dimension of this nullspace, we can let $y = Nx$ where the k columns of N span $\mathcal{N}(A)$. (Note that x does not refer to reactance in this context.) This change of variables is akin to a rotation, but reduces the problem dimension to k. Partitioning N according to,

$$\begin{bmatrix} y_1 \\ y_2 \\ y_3 \end{bmatrix} = \begin{bmatrix} N_1 \\ N_2 \\ N_3 \end{bmatrix} x$$

allows (4) to be written,

$$\begin{aligned} \min \quad & x^\top (N_1^\top Q_z N_1) x + 2 x^\top (N_1^\top Q_z z_1^*) && \text{(5a)} \\ s.t. \quad & x^\top N_3^\top N_3 x = c. && \text{(5b)} \end{aligned}$$

All feasible solutions to (5) lie in the nullspace of A, so the linear constraints are now implicit.

C. Obtaining a norm constraint

After kernel mapping, the quadratic constraint is no longer a norm constraint. This can be corrected in two steps. First, perform an eigendecomposition $N_3^\top N_3 = U D U^\top$ and let $\hat{x} = U^\top x$. The constraint is diagonal in terms of $\hat{x}$:

$$x^\top N_3^\top N_3 x = \hat{x}^\top D \hat{x} \tag{6}$$

where D is diagonal and has at most T nonzero elements, so the right side of (6) may be expanded into:

$$\begin{bmatrix} \hat{x}_1^\top & \hat{x}_2^\top \end{bmatrix} \begin{bmatrix} 0 & 0 \\ 0 & \hat{D} \end{bmatrix} \begin{bmatrix} \hat{x}_1 \\ \hat{x}_2 \end{bmatrix}. \tag{7}$$

The second step is to change variables from $\hat{x}$ to $w = [w_1^\top \; w_2^\top]^\top$. The variables x, $\hat{x}$ and w are related through:

$$\begin{aligned} \begin{bmatrix} w_1 \\ w_2 \end{bmatrix} = \begin{bmatrix} I & 0 \\ 0 & \hat{D}^{1/2} \end{bmatrix} \begin{bmatrix} \hat{x}_1 \\ \hat{x}_2 \end{bmatrix} = K \hat{x} \qquad \text{(8)} \\ \implies w = K U^\top x. \end{aligned}$$

(Note that $x = U K^{-1} w$ because $U U^\top = I$.) In terms of w, (5b) is transformed through (6) to give the form of a norm:

$$\hat{x}^\top D \hat{x} = \hat{x}_2^\top \hat{D}^{1/2} \hat{D}^{1/2} \hat{x}_2 = w_2^\top w_2 \; . \tag{9}$$

Of course, this change of variables must also be applied to the cost function. After substitution and simplification, the full problem becomes:

$$\begin{aligned} \min \quad & w^\top B w + w^\top b && \text{(10a)} \\ s.t. \quad & w_2^\top w_2 = c && \text{(10b)} \end{aligned}$$

where

$$B = K^{-1} U^\top N_1^\top Q_z N_1 U K^{-1} \text{ and } b = 2 K^{-1} U^\top N_1^\top Q_z z_1^*.$$

The manipulations in this section have restored the norm structure of the quadratic constraint. In the next section we use the KKT conditions of (10) to eliminate w_1, the unconstrained part of w. This will allow us to write the objective in terms of w_2 only.

D. Eliminating w_1

Note that w_1 is unconstrained in (10). For a fixed w_2, we can use the KKT conditions to find w_1 such that the objective is minimized. Begin by expanding the objective:

$$\begin{aligned} f(w) &= \begin{bmatrix} w_1^\top & w_2^\top \end{bmatrix} \begin{bmatrix} B_{11} & B_{12} \\ B_{12}^\top & B_{22} \end{bmatrix} \begin{bmatrix} w_1 \\ w_2 \end{bmatrix} + \begin{bmatrix} w_1^\top & w_2^\top \end{bmatrix} \begin{bmatrix} b_1 \\ b_2 \end{bmatrix} \\ &= w_1^\top B_{11} w_1 + 2 w_1^\top B_{12} w_2 + w_2^\top B_{22} w_2 \\ &\quad + w_1^\top b_1 + w_2^\top b_2. \end{aligned}$$

Next, set the partial derivative with respect to w_1 equal to zero:

$$\begin{aligned} \frac{\partial f}{\partial w_1} &= 2 w_1^\top B_{11} + 2 w_2^\top B_{12}^\top + b_1^\top = 0 \\ \implies w_1 &= -B_{11}^{-1} \left(B_{12} w_2 + \frac{1}{2} b_1 \right). \end{aligned} \tag{11}$$

After substitution of (11), the objective depends only on w_2:

$$f(w_2) = w_2^\top \left(B_{22} - B_{12}^\top B_{11}^{-1} B_{12}\right) w_2 + w_2^\top (b_2 - B_{12}^\top B_{11}^{-1} b_1).$$

(Note that the constant term, which plays no role in minimization, was omitted.) The full optimization problem becomes:

$$\min \quad w_2^\top \hat{B} w_2 + w_2^\top \hat{b} \tag{12a}$$

$$s.t. \quad w_2^\top w_2 = c, \tag{12b}$$

where

$$\hat{B} = B_{22} - B_{12}^\top B_{11}^{-1} B_{12} \text{ and } \hat{b} = b_2 - B_{12}^\top B_{11}^{-1} b_1.$$

This is a QCQP in T dimensions with a single norm constraint. It is straightforward to obtain solutions to this problem, as the next subsection shows.

E. Solution via enumeration

A straightforward method of solving (12) involves initially diagonalizing $\hat{B}$ through an eigendecomposition. It will be assumed that step has been completed. Let v be the Lagrange multiplier associated with (12b) and write the first-order optimality condition for (12):

$$\frac{\partial \mathcal{L}(w_2, v)}{\partial w_2} = 2\hat{B} w_2 + \hat{b} - v(2w_2) = 0$$

$$\implies \hat{B} w_2 + \frac{1}{2}\hat{b} = v w_2 \ . \tag{13}$$

Equation (13) is a linear system that yields w_2 for fixed v:

$$w_{2,i} = \frac{\hat{b}_i/2}{v - \hat{B}_{i,i}} \ . \tag{14}$$

In addition to satisfying (14), an optimal w_2 must satisfy the quadratic constraint. Substituting (14) into (12b) yields the "secular equation" (see [10]):

$$s(v) = \sum_i \left(\frac{\hat{b}_i/2}{v - \hat{B}_{i,i}} \right)^2 = c. \tag{15}$$

Note that $s(v)$ has one pole per unique nonzero diagonal element of $\hat{B}$. There are at most two solutions per pole, one on each side. This is best understood graphically. Figure 2 illustrates a three-pole secular equation taken from analysis of the RTS-96 network. The Lagrange multiplier v is on the horizontal axis, and the secular equation value $s(v)$ is on the vertical. Solutions are intersections of $s(v)$ with the horizontal line $s(v) = c$. They can be computed numerically with a simple binary search algorithm.

V. Implementation details

No iterative scheme is required to solve the temporal instanton QCQP; only a string of transformations is required. Still, thorough analysis requires a QCQP solution for each line in the network. As the number of lines and nodes increases, processing and memory requirements grow quickly. Careful implementation is required to make the method scale well.

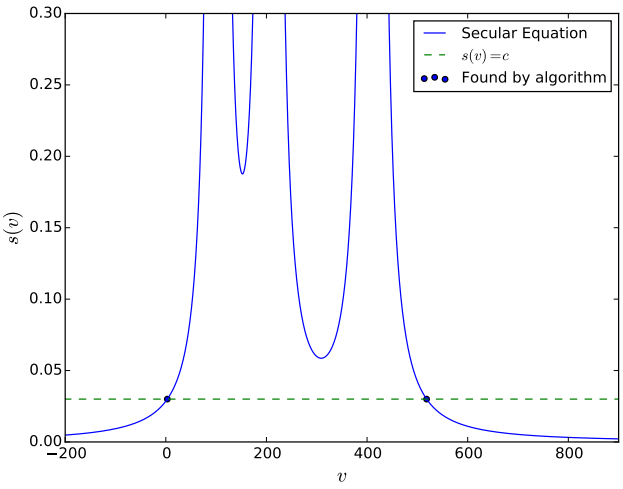

Fig. 2. Plot of secular equation for a single line in the RTS-96. Note that $s(v)$ approaches infinity at the three poles, and there could be as many as six solutions if c were large enough.

- Use sparse methods to build QCQP matrices. This makes a dramatic difference in storage requirements. As an example, the Q_θ matrix for RTS-96 temporal instanton analysis with six time intervals requires 2.5 MB in dense form; a sparse representation occupies just 40 bytes.
- Use sparse methods for matrix multiplication, concatenation, and factorization. Maintain sparsity from start to finish. Any step that uses a dense matrix representation will be a bottleneck, especially for larger networks.
- Parallelize. After the unchanging pieces of QCQP are built, the remainder of analysis consists of building smaller matrices and performing various transormations for each line in the network. Each line's analysis is independent from all others, so a parallel for loop is a great way to spread computation across multiple processors. After experimenting with anywhere from one to five worker processes on a four-core laptop, we decided that the best processing time/memory allocation tradeoff is to use two processors. This cut overall computation time in half with just a modest increase in memory allocation.

Translation, the first step of the QCQP solution method, is computationally expensive and relies on the A matrix having full row rank. Unfortunately, A can have linearly dependent rows for some lines in certain networks.

VI. Results

We used data from [11] to demonstrate temporal instanton analysis on a wind-augmented RTS-96 network model.

VII. Conclusions

VIII. Appendix: line temperature model

A. The heat balance equation

The change in temperature of any object may be expressed as a differential equation called the heat balance equation, which relates temperature change to a sum of various sources

of heating. The IEEE 738 standard [8] provides the following heat balance equation for a transmission line:

$$\frac{dT}{dt} = \frac{1}{m \cdot C_p}\left[I^2 \cdot R(T) - q_c - q_r + q_s\right] \tag{16}$$

where

- T is the conductor average temperature.
- $m \cdot C_p$ is the product of mass and heat capacity.
- $I^2 \cdot R(T)$ represents heat rate due to resistive heating. In this paper the term is replaced by f_{ij}^{loss}, the DC approximate line loss expression derived in [9]:

$$f_{ij}^{\text{loss}} \approx r_{ij}\left(\frac{\theta_{ij}}{x_{ij}}\right)^2, \tag{17}$$

  where θ_{ij} is the difference between angles θ_i and θ_k, and $r_{ij} + jx_{ij}$ is the impedance of the line between nodes i and j. Three assumptions underpin (17): voltage magnitudes are all 1 pu, cosine may be approximated by its second-order Taylor expansion, and $x_{ij} \geq 4r_{ij}$. Thus, (17) uses DC power flow assumptions to approximate line losses, but remains nonlinear.
- q_c is the rate of heat loss due to convection. Any object at a higher temperature than surrounding air will gradually cool as the air carries heat away. This phenomenon is proportional to the temperature difference between the line and surrounding air:

$$q_c = \eta_c \cdot (T - T_{\text{amb}}) \ , \tag{18}$$

  where T_{amb} is the ambient temperature (of surrounding air).
- q_r is the rate of heat loss due to radiation. Thermal radiation is the process by which thermal energy is converted to electromagnetic energy in all objects with non-zero absolute temperature. It is modeled by a fourth-order expression:

$$q_r = \eta_r \cdot \left[(T + 273)^4 - (T_{\text{amb}} + 273)^4\right] \tag{19}$$

- q_s is the rate of heat gain due to solar heating. In this paper the solar heat rate is fixed to some conservative constant (representing full direct sun), but it is important to note that solar heat rate varies significantly with cloud cover, geometry, and even insulation type (reflective versus black).

B. Linearization of radiation heat rate

When (16) is combined with an initial temperature T_0, the resulting initial value problem makes it possible to determine the temperature at any later time. We substitute (18) and (19) into (16) and attempt to solve for temperature:

$$\frac{dT}{dt} = \frac{1}{mC_p}\big[f_{ij}^{\text{loss}} - \eta_c\left(T(t) - T_{\text{amb}}\right) - \eta_r\left((T(t) + 273)^4 - (T_{\text{amb}} + 273)^4\right) + q_s\big] \tag{20}$$

Suppose that power flow, ambient temperature, and solar heat rate are constant during a temperature change calculation. Then there are just two variable terms on the right-hand side: one first-order and the other fourth-order. The fourth-order term (which comes from q_r) makes this equation difficult to solve. Fortunately, q_r is approximately linear over the temperature range we are interested in (from ambient temperature to temperature limit). We replace q_r by $\tilde{q}_r$, a conservative[2] linearization:

$$\tilde{q}_r = \eta_r\left((T_{\text{mid}} + 273)^4 - (T_{\text{amb}} + 273)^4\right) + 4\eta_r(T_{\text{mid}} + 273)^3 \cdot (T(t) - T_{\text{mid}}) \tag{21}$$

C. Line temperature as recursive relationship

Substitution of (21) into (20) yields the approximate heat balance equation

$$\frac{dT}{dt} = aT(t) + b \ , \tag{22}$$

where constants a and b are defined as

$$a = \frac{1}{mC_p}\left[-\eta_c - 4\eta_r(T_{\text{mid}} + 273)^3\right] \tag{23a}$$

$$b = \frac{1}{mC_p}\big[f_{ij}^{\text{loss}} + \eta_c T_{\text{amb}} - \eta_r\big((T_{\text{mid}} + 273)^4 - (T_{\text{amb}} + 273)^4\big) + 4\eta_r T_{\text{mid}}(T_{\text{mid}} + 273)^3 + q_s\big] \tag{23b}$$

Our approximate heat balance initial value problem (22) has a straightforward solution:

$$T(t) = ke^{at} - \frac{b}{a} \tag{24}$$

where $k = T(0) + b/a$. Note that b is influenced by power flow (via f_{ij}^{loss}), but a is not.

The only variables in (24) are initial temperature and angle differences during each time interval. There is therefore a recursive relationship between final temperature and initial temperature that involves only angle differences. The derivation of this recursive relationship is an exercise in messy linear algebra; it is omitted here for brevity.

References

[1] M. Chertkov, F. Pan, and M. Stepanov, "Predicting failures in power grids: The case of static overloads," *IEEE Transactions on Smart Grid*, vol. 2, no. 1, pp. 162–172, Mar. 2011.

[2] M. Chertkov, M. Stepanov, F. Pan, and R. Baldick, "Exact and efficient algorithm to discover extreme stochastic events in wind generation over transmission power grids," in *Proc. 2011 50th IEEE Conference on Decision and Control and European Control Conference (CDC-ECC)*, 2011, pp. 2174–2180.

[3] S. Baghsorkhi and I. Hiskens, "Analysis tools for assessing the impact of wind power on weak grids," in *Proc. Systems Conference (SysCon), 2012 IEEE International*, 2012, pp. 1–8.

[4] H. Banakar, N. Alguacil, and F. Galiana, "Electrothermal coordination part I: theory and implementation schemes," *IEEE Transactions on Power Systems*, vol. 20, no. 2, pp. 798–805, May 2005.

[5] "IEEE standard for calculating the current-temperature of bare overhead conductors," *IEEE Std 738-2006 (Revision of IEEE Std 738-1993)*, pp. c1–59, Jan. 2007.

[2] Because a transmission line is hotter than surrounding air, radiation tends to decrease line temperature. Thus, a conservative approach will underestimate the radiation heat rate, leading to slightly higher temperatures.

TABLE I
LINE HEATING PARAMETERS

Parameter	Units	Description
T_s	s	Sample time
mC_p	$J/(m \cdot C)$	Per-unit-length heat capacity of the conductor
η_c	$W/(m \cdot C)$	Conductive heat loss rate coefficient
η_r	$W/(m \cdot C)$	Radiative heat loss rate coefficient
T^{lim}	C	Line temperature at steady-state current limit.
$\Delta q_{s,ij}$	W/m	Solar heat input into conductor
ΔT_{amb}	C	Change in ambient temperature

[6] B. Hodge and M. Milligan, "Wind power forecasting error distributions over multiple timescales," in *2011 IEEE Power and Energy Society General Meeting*, Jul. 2011, pp. 1–8.

[7] J. Tastu, P. Pinson, and H. Madsen, "Space-time trajectories of wind power generation: Parameterized precision matrices under a Gaussian copula approach," in *Modeling and Stochastic Learning for Forecasting in High Dimensions*, ser. Lecture Notes in Statistics, X. Brossat, Ed. Springer, 2015, pp. 267–296.

[8] "IEEE Standard for Calculating the Current-Temperature Relationship of Bare Overhead Conductors," *IEEE Std 738-2012 (Revision of IEEE Std 738-2006 - Incorporates IEEE Std 738-2012 Cor 1-2013)*, pp. 1–72, Dec. 2013.

[9] M. Almassalkhi and I. Hiskens, "Model-predictive cascade mitigation in electric power systems with storage and renewables – part I: Theory and implementation," *IEEE Transactions on Power Systems*, vol. PP, no. 99, pp. 1–11, 2014.

[10] D. Bienstock and A. Michalka, "Polynomial Solvability of Variants of the Trust-region Subproblem," in *Proceedings of the Twenty-Fifth Annual ACM-SIAM Symposium on Discrete Algorithms*, ser. SODA '14. Portland, Oregon: SIAM, 2014, pp. 380–390. [Online]. Available: http://dl.acm.org/citation.cfm?id=2634074.2634102

[11] H. Pandzic, Y. Dvorkin, T. Qiu, Y. Wang, and D. Kirschen. Unit Commitment under Uncertainty - GAMS Models, Library of the Renewable Energy Analysis Lab (REAL), University of Washington, Seattle, USA. [Online]. Available: http://www.ee.washington.edu/research/real/gams_code.html

[12] O. Mehanna, K. Huang, B. Gopalakrishnan, A. Konar, and N. Sidiropoulos, "Feasible point pursuit and successive approximation of non-convex QCQPs," *IEEE Signal Processing Letters*, vol. PP, no. 99, pp. 1–1, 2014.